H-T magnetic phase diagrams of electron-doped $Sm_{1-x}Ca_xMnO_3$: Evidence for phase separation and metamagnetic transitions

M. Respaud* and J. M. Broto
Laboratoire de la Physique de la Matière Condensée, INSA, Complexe Scientifique de Rangueil, 31077 Toulouse Cedex, France

H. Rakoto
Laboratoire National des Champs Magnétiques Pulsés, INSA, Complexe Scientifique de Rangueil, 31077 Toulouse Cedex, France

J. Vanacken and P. Wagner
Laboratorium voor Vaste-Stoffysica en Magnetisme, Katholieke Universiteit Leuven, Celestijnenlaan 200 D, 3001 Leuven, Belgium

C. Martin, A. Maignan, and B. Raveau
Laboratoire CRISMAT, UMR No. 6508, ISMRA, Boulevard du Maréchal Juin, 14050 Caen, France
(Received 1 August 2000; published 22 March 2001)

The magnetic properties of the polycrystalline manganites $Sm_{1-x}Ca_xMnO_3$ have been studied for ($1 \geqslant x \geqslant 2/3$) under high magnetic fields up to 50 T. The phase diagrams in the H-T plane have been determined. The more representative systems have also been studied by means of neutron diffraction experiments. Increasing the electron concentration in $CaMnO_3$ leads to an increasing minor ferromagnetic (FM) component superimposed on the antiferromagnetic (AFM) background. A cluster-glass regime is observed for $x=0.9$, where FM clusters are embedded in the G-type AFM matrix of the parent compound. For $0.8 \geqslant x$, field-induced transitions from the AFM ground state to a FM one have been observed. They correspond to the melting of the C-type AFM orbital-ordered phase for $x=0.8$, and to the collapse of the charge-ordered phase for $x=3/4$. In between these two characteristic domains of concentration, $x \sim 0.85$, the magnetization curves show a superposition of the two above behaviors, suggesting phase separation. This scenario is consistent with the neutron diffraction results showing that the crystalline and magnetic structures of each phase coexist.

DOI: 10.1103/PhysRevB.63.144426 PACS number(s): 75.25.+z, 75.30.Kz, 75.30.Vn

I. INTRODUCTION

The recent reinvestigation of Mn perovskites has revealed their amazing physical properties, among them, colossal magnetoresistance (CMR), charge ordering, orbital ordering, and phase separation.[1–4] These properties can be tuned by changing the nature and the concentrations of the trivalent rare-earth and divalent alkaline-earth cations, which determine both the distortion of the crystalline structure and the concentration of e_g electrons at the Mn sites. As the average size of the cations at the lanthanide sites is reduced, a tilt of the MnO_6 octahedra is induced, which favors the localization and ordering of the Mn^{3+}/Mn^{4+} cations. Beside the double-exchange (DE) interactions inducing a ferromagnetic (FM) metallic ground state,[5] long-range Coulomb repulsion and Jahn-Teller distortion favor the localization of the Mn^{3+} and Mn^{4+} species and the antiferromagnetic (AFM) coupling of their magnetic moments. The interplay between charge, spin, lattice, and orbital degrees of freedom is the source of the very rich phase diagram.

Among the variety of these phases, one of the most original results concerns the observation of long-range charge ordering (CO) for equal concentrations of Mn^{3+} and Mn^{4+} species, e.g., $Nd_{1/2}Sr_{1/2}MnO_3$ or $R_{1/2}Ca_{1/2}MnO_3$ (R = La, Pr, Nd, Sm).[6–9] In this state, an ordering of the $d_{3z^2-r^2}$ orbitals, as well as the carriers, occurs. As a consequence, the Mn magnetic moments adopt a CE-type AFM structure at low temperature. More generally, CO is commonly observed when the nominal carrier concentration takes an integer or commensurate value, e.g., $x=1/2,2/3,3/4$ for $L_{1-x}Ca_xMnO_3$ (L is a lanthanide).[10–15] These CO phases are relatively unstable since they can be melted by several physical excitations. In particular, the application of a magnetic field drives the insulator (I) CO phase into a FM metallic (M) state.[10,11] In the case of the $L_{1/2}Ca_{1/2}MnO_3$ series, the strength of the field needed for the melting increases when the one-electron bandwidth of the material is reduced. Another originality of these manganites concerns precisely the inhomogeneous electronic and magnetic properties, observed, for example, in $Pr_{2/3}Ca_{1/3}MnO_3$.[16,17]

Systematic investigation of the electron-doped part of the phase diagram has started very recently. It has been performed on several compounds, especially on the $Sm_{1-x}Ca_xMnO_3$ series.[13,15] Upon increasing the electronic concentration, the insulating AFM G-type $CaMnO_3$ adopts a metalliclike behavior within a cluster-glass (CG) magnetic ground state ($x \approx 0.9$). Then it transforms to an insulator AFM CO state for $x \leqslant 0.8$. At the boundary of theses two phases ($x \approx 0.85$), CMR was observed in fields below 7 T. The presence of CO phases for $0.8 \geqslant x \geqslant 0.5$ is a common feature of several systems with La, Pr, or Bi at the L^{3+} site.[13–15,18] Most of the experiments were devoted to determination of the real electronic and magnetic order in the CO phases which are still under discussion. For L = La, low-temperature electron diffraction and high-resolution images from electron microscopy revealed the presence of charge-

ordered stripes for $x=2/3$ and $3/4$.[19] More recently, high-magnetic-field magnetization measurement studies showed the melting of the CO phase in $Bi_{0.25}Ca_{0.75}MnO_3$.[20] The evolution of these CO systems toward the parent compound $CaMnO_3$ on reducing the electronic concentration is not well understood.

Our paper deals with investigation of the magnetic properties of the electron-doped perovskite manganite by using high magnetic fields. Starting from the parent compound $CaMnO_3$, doping was achieved by substituting Sm^{3+} for Ca^{2+}. The detailed electron diffraction and lattice imaging studies as well as the magnetic and transport properties up to 5 T have been described elsewhere.[13,14,21] Isothermal magnetization measurements $[M(H)]$ were performed in pulsed magnetic fields up to 50 T between 4 K and room temperature. These measurements combined with neutron diffraction experiments allow us to complete the *H-T* magnetic phase diagram of the electron-doped $Sm_{1-x}Ca_xMnO_3$ compounds. Three classes of behavior can be distinguished. Upon doping $CaMnO_3$ $(x=1)$ up to 10% $(x=0.9)$, the $M(H)$ curves evolve from those of a pure AFM to a more complex behavior with a low-field FM component superimposed on the AFM contribution. For $x\leqslant 0.8$, metamagnetic transitions from the AFM ground state to a FM state are evident. At the boundary of these two domains, for $x\sim 0.85$, the $M(H)$ curves exhibit the superposition of the $x\geqslant 0.9$ and $x\leqslant 0.8$ different behaviors, suggesting the occurrence of phase-separation phenomena.

II. EXPERIMENTAL RESULTS

Polycrystalline samples were synthesized using stoichiometric mixtures of Sm_2O_3, CaO, and Mn_2O_3 compounds as previously described.[22–24] The mixtures with nominal compositions $Sm_{1-x}Ca_xMnO_3$ were first heated at 1000 °C to achieve decarbonation, sintered at 1500 °C for 12 h, slowly cooled down to 800 °C, and then quenched to room temperature. Purity and cationic homogeneity were systematically checked by x-ray and electron diffraction coupled with energy-dispersive spectroscopy analysis.

The main high-magnetic-field measurements were performed using the facilities developed by the LNCMP in Toulouse (France). Using the discharge of a bank capacitor in a coil, pulsed fields up to 35 T are obtained. The field increases according to a sinusoidal law, reaching its maximum after 0.1 s, and then decreases to zero with an exponential shape during 1.4 s. Some measurements were carried out using the facilities developed by the LVSM in Leuven (Belgium) where 50 T is available, but with a pulse duration of 20 ms. The magnetization was measured by inductive methods using a system of two concentric compensated pick-up coils in opposition. The measured signal dM/dt is then integrated numerically. All the measurement were systematically performed after zero-field cooling from room temperature down to the temperature of measurement, in order to avoid any metastable state. The measurements were done during increasing and decreasing field to get the rising- and lowering-field branches of the $M(H)$ curves.

The evolution with electronic concentration of the isothermal $M(H)$ curves under high magnetic fields up to 35 T measured at low temperature $(T=4.2\ \mathrm{K})$ is presented in Fig. 1. The parent compound $CaMnO_3$ clearly shows classical AFM behavior. Doping it with electrons is sufficient to induce a partial FM polarization M_0 (see the lowest part of Fig. 1). The low-temperature $M(H)$ curves are thus composed of a FM component followed by a linear increase of the magnetization, characteristic of an AFM contribution. No hysteresis was evidenced in the sweep-up and -down processes. The FM correlations reach their maximum intensity in the vicinity of $x=0.88-0.9$. For these samples, upon warming, the FM component vanishes above the magnetic ordering temperature and pure paramagnetic (PM) behavior is observed at higher temperatures.

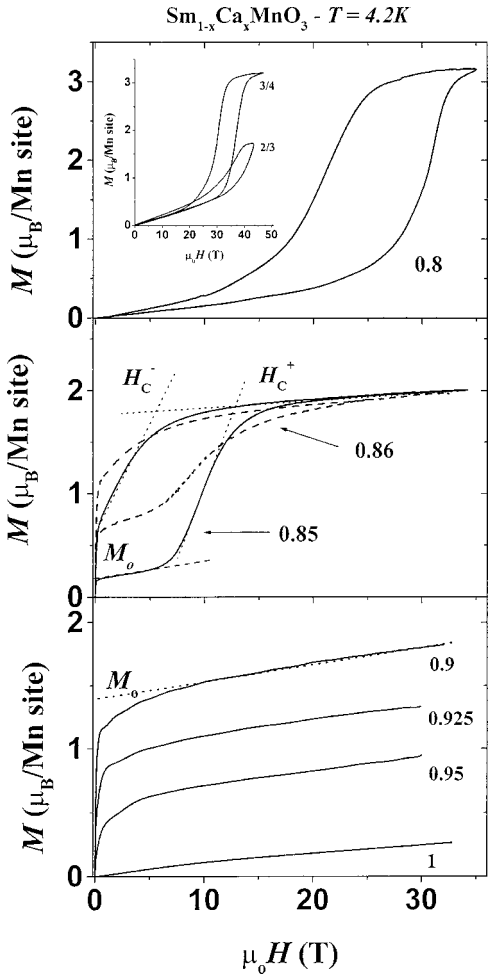

FIG. 1. Magnetization curves of $Sm_{1-x}Ca_xMnO_3$ measured at 4.2 K, for different x values (mentioned on each curve). All these curves were recovered during the sweep up and down of the pulsed magnetic field after zero-field cooling. No hysteresis was evidenced. The plots also show how the critical fields (H_C^+ and H_C^-) and the FM component M_0 were estimated.

Further increase of the electronic concentration results again in a pure AFM ground state $(0.8\geqslant x)$. As shown in the top part of Fig. 1, the magnetic behavior under magnetic field differs drastically from the previous cases. For the $x=0.8$ compound, the magnetization process presents a sharp step characteristic of a metamagnetic transition from the ini-

tial AFM state to a final FM one, with a wide hysteresis in the sweep-up and -down processes. The magnetization reaches the expected theoretical value in the case of a fully FM polarization of the Mn magnetic moments, just above $3\mu_B$ per Mn site. The magnetic contribution of the Sm^{3+} sublattice is difficult to estimate since the magnetization is not saturated. However, it should be minor and behave as a PM as in the case of $Sm_{1/2}Ca_{1/2}MnO_3$. Upon warming, the $M(H)$ curves exhibit similar shapes with decreasing critical fields. Finally, the metamagnetic transition disappears for temperatures above T_N, which also corresponds to the metal-insulator transition. Although the behavior of the $x=3/4$ compound is similar, its critical fields are higher. For the $x=2/3$ compound, 45 T was not sufficient to observe the complete metamagnetic transition. Since the two adjacent charge-ordered compounds with $x=3/4$ and 1/2 exhibit a complete transition toward a fully FM polarization, we may expect similar phenomena for $x=2/3$ in fields in the range of 50–70 T.

At intermediate concentrations $0.8<x<0.88$, another magnetic behavior is evident. The intermediate plot of Fig. 1 presents the $M(H)$ curves measured at low temperature for $x=0.86$ and 0.85. These curves combine the two magnetization processes aforementioned: an FM component, followed by a metamagnetic transition, and finally a linear increase of the magnetization in higher magnetic fields. The magnetization value for $\mu_0 H=30$ T is around $2\mu_B$ per unit cell, far below the theoretical saturation value. It should be noted that the FM component is less important for $x=0.85$ than for $x=0.86$ but the magnetization step is broader. The two concomitant phenomena indicate that the FM is strongly decreasing for this range of carrier concentration, before the establishment of another pure AFM state at higher concentration ($x=0.8$). Similar magnetization features have been observed at higher temperatures, until the magnetic ordering temperature is reached. The magnitude of the magnetization jump remains essentially constant in the whole temperature range.

These magnetic measurements allow us to determine the *H-T* phase diagrams of these electron-doped manganites. Concerning the metamagnetic transitions, the critical fields, denoted $H_c^+(H_c^-)$ for the first (remanent) magnetization have been defined by extrapolating the magnetization step and the saturation plateau (see the intermediate plot of Fig. 1 which illustrates the graphic construction). The corresponding *H-T* phase diagrams are given in Fig. 2. The thermodynamic transition fields defined as $H_c=(H_c^+ + H_c^-)/2$ are indicated on the phase diagrams. For the sake of conciseness, the $x=0.86$ curve is not shown since the critical fields and temperature dependence are very close to the values found for $x=0.85$.

For a better understanding of the evolution of the magnetic properties with the electron concentration, the peculiar crystalline and magnetic microstructures of the three regimes $x=0.8$, 0.85, and 0.9 have been investigated by means of neutron diffraction (ND). ND experiments were carried out at the LLB (Saclay, France) on the G41 diffractometer using the wavelength $\lambda=2.4266$ Å. Some of them have been described in detail elsewhere.[25,26] All these compounds exhibit the *Pnma* structure in the paramagnetic state at room temperature. At low temperature, $Sm_{0.1}Ca_{0.9}MnO_3$ is still characterized by the *Pnma* space group (see Fig. 3). Although, at low temperature, a unique nuclear structure is observed, the magnetic one is phase separated. It consists of FM regions embedded in a *G*-type AFM matrix.[26] These zones created by Mn^{3+} injection allow DE interactions to take place. The metallicike behavior observed below T_N is established through FM region percolation.[26] The average magnetic moment at 4.2 K determined for the AFM phase, from the neutron study, is $\mu(G)=2.1\mu_B$ and for the FM region $\mu(F)=1.17\mu_B$. The latter estimation is in rather good agreement with our magnetization data.

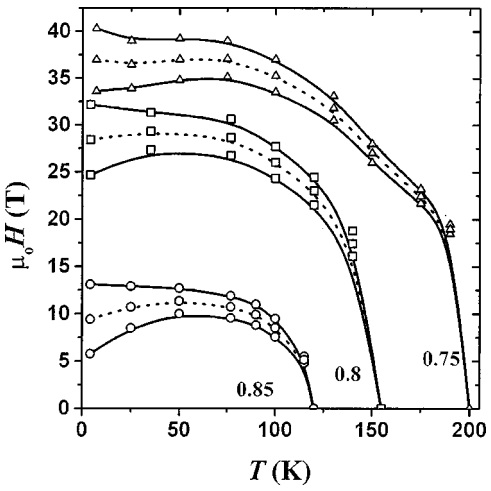

FIG. 2. *H-T* phase diagrams of the metamagnetic samples of $Sm_{1-x}Ca_xMnO_3$ with $x=0.75$, 0.8, and 0.85, deduced from the $M(H)$ curves. For each compound, the upper (lower) curve corresponds to the critical field $H_C^+(H_C^-)$ of the metamagnetic transition in the sweep-up (-down) process. The dotted line presents the thermodynamic field $H_C=(H_C^+ + H_C^-)/2$.

On the other hand, the low-temperature crystalline structure of $Sm_{0.2}Ca_{0.8}MnO_3$ presents a monoclinic distortion below 150 K, characterized by the $P2_1/m$ space group. The

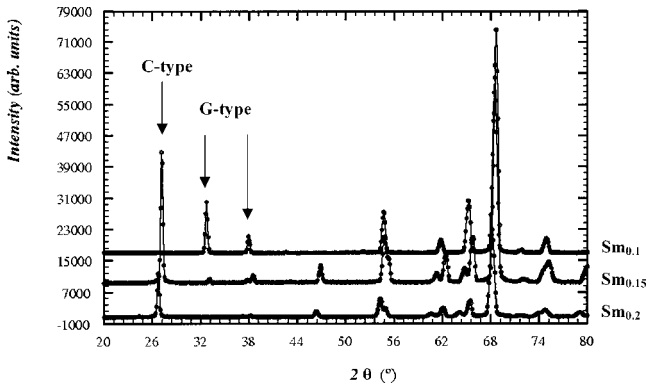

FIG. 3. Neutron diffraction patterns collected at 2 K for three characteristic compounds with $x=0.8(Sm_{0.2})$, $0.85(Sm_{0.15})$, and $0.9(Sm_{0.1})$. *C*-type and *G*-type AFM is associated with the $P2_1/m$ and *Pnma* crystalline structures, respectively.

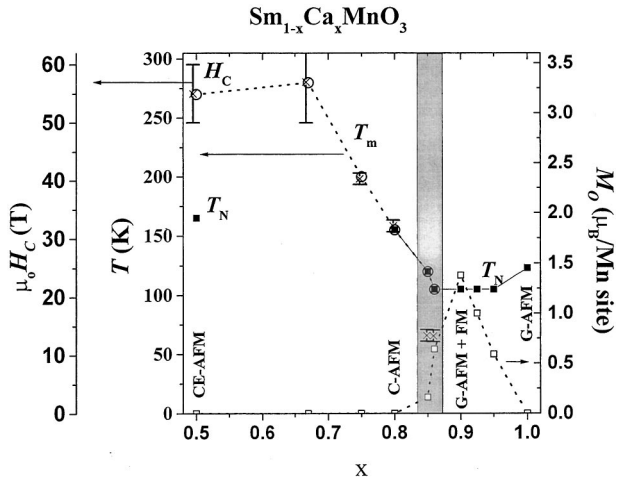

FIG. 4. Evolution of magnetic properties with the electronic concentration (x). M_0 (open square), FM component measured at 4.2 K; T_N (dark square), Néel temperature; T_m (open circle), temperature at which the metamagnetic transition occurs. H_C^+ (cross and error bar), thermodynamic field of the metamagnetic transition measured at 4.2 K on the ascending branch. The H_C^+ and T_m scales have been adapted in order to show their proportionality in the OO domain. Data from Ref. 9 for $x=0.5$ are also included. Lines are just guides to the eye. The gray area indicates the intermediate zone where phase separation occurs.

$d_{3z^2-r^2}$ orbitals are ordered into chains along the pseudotetragonal axis, which leads to a *C*-type AFM structure.[27] A study by electron microscopy at 90 K reveals the occurrence of long-range CO for $Sm_{0.25}Ca_{0.75}MnO_3$ with $T_{CO} \sim T_N$.[13]

As shown in Fig. 3, at low temperature, the intermediate compound $Sm_{0.15}Ca_{0.85}MnO_3$ presents unambiguous phase separation where the ND patterns consist of a linear combination of both $Sm_{0.1}Ca_{0.9}MnO_3$ and $Sm_{0.2}Ca_{0.8}MnO_3$ spectra, with a large majority of the $P2_1/m$ *C*-type phase (94%).[25] Preliminary ND experiments under magnetic fields show that the ratio between the two nuclear phases (*Pnma* and $P2_1/m$) is sensitive to the applied magnetic field. For $\mu_0 H=6$ T and $T=100$ K, the sample is transformed into a majority *Pnma* phase (56%), and it retains only 44% of the $P2_1/m$ phase. A similar phenomenon is induced by high magnetic fields at low temperature.

III. DISCUSSION AND CONCLUDING REMARKS

The present experimental study enables us to complete the phase diagram of the electron-doped $Sm_{1-x}Ca_xMnO_3$ systems by extending it toward high magnetic fields. The main physical parameters are thus summarized in Fig. 4. Data from Ref. 9 have also been included in order to complete this study up to $x=0.5$. The low-field FM contribution (M_0), the transition field of the rising branch (H_c^+) measured at $T=4.2$ K, and the magnetic ordering temperature (T_N) are compiled as functions of x. For metamagnetic systems, the temperatures at which the metamagnetic transition starts to occur are reported (T_m). They also correspond to the *M-I* transition temperature (T_{MI}). Finally, the low-temperature magnetic ground states determined by means of ND are also indicated.

Starting from the insulating *G*-type AFM $CaMnO_3$ parent compound, its doping with electrons leads to a growing FM component. The maximum intensity is obtained for $x \sim 0.1-0.12$. The matrix still keeps the *G*-type AFM. The magnetization data do not allow us to identify the origin of the FM component; maybe it is due to canting or to the presence of FM clusters. However, considering the percolative nature of the resistivity, the second hypothesis is more probable, suggesting a cluster-glass regime.[24]

On the other hand, for $x=3/4$ and 0.80, metamagnetic transitions from AFM to complete FM ordering of the Mn spins are observed. A similar behavior has also been shown for $x=1/2$, while it is incomplete for $x=2/3$ in fields below 45 T. Along that set of concentrations, the nature of the field-induced transition evolves. For $x=1/2$, the metamagnetic transition corresponds to the melting of the CO with CE-AFM order. For $x=0.8$, only orbital ordering occurs with a polarization of the $d_{3z^2-r^2}$ orbital into chains along the pseudotetragonal axis leading to *C*-type AFM. With such orbital ordering (OO); the carriers move along the chains. To the best of our knowledge, this is the first observation of the melting of OO with *C*-type AFM. It corresponds to the third kind of metamagnetic transition, after the melting of CO with CE-type AFM of $L_{1/2}Ca_{1/2}MnO_3$ and $Nd_{1/2}Sr_{1/2}MnO_3$ compounds where the electrons are localized, and the melting of the $d_{x^2-y^2}$ OO phase with *A*-type AFM in $Pr_{1/2}Sr_{1/2}MnO_3$, where the electrons are confined in planes. Between $x=0.8$ and 1/2, the way OO evolves with the electron concentration has to be clarified.

In Fig. 4, the T_m and H_c^+ scales have been adapted in order to show their proportionality and identical dependence vs x. An estimation of H_c^+ for $x=2/3$ gives 55–60 T. One should remark that $k_B T_m$ is approximately two times bigger than $\mu_0 \mu_{Mn} H_c^+$, where μ_{Mn} is the average magnetic moment per Mn site. This difference in the energies involved in the melting of CO phases has been observed in other CO systems. In fact, the high-field FM polarization should also induce a metallic behavior as in $Nd_{1/2}Sr_{1/2}MnO_3$, as well as a structural transition, which also gives an energizing contribution.[28]

The last part of the phase diagram concerns the intermediate concentration area with $0.8<x<0.88$. Both the magnetization data and the ND patterns evidence the mixing of the two nearest phases at low temperature. The crystalline and associated magnetic structures, namely, the $P2_1/m$ and *Pnma* space groups associated with *C*-type AFM and FM with *G*-type AFM of $Sm_{0.2}Ca_{0.85}MnO_3$ and $Sm_{0.1}Ca_{0.85}MnO_3$, respectively, coexist. The $M(H)$ behavior is just the consequence of this phase mixing. From our $M(H)$ data, considering that the magnetization is fully polarized after the metamagnetic transition as for $x=0.75-0.8$, we can estimate the contribution of the OO phase, in the range of roughly 50%, which is in good agreement with ND data under magnetic fields. Our data also show that the transition from the CG to the OO regime is progressive. Indeed, the magnetization curves show the pro-

gressive reduction of the FM component with a concomitant increase of the metamagnetic step amplitude as the electron concentration increases.

As compare to single-phase OO systems, one should notice that the ratio between $\mu_0\mu_{\mathrm{Mn}}H_c^+$ and k_BT_m energies is lower, suggesting the peculiar instability of the OO phase. The $M(H)$ curves are very reminiscent of those published for $Pr_{2/3}Ca_{1/3}MnO_3$.[29] This latter compound also presents phase separation at low temperature where FM clusters are embedded in a CO AFM matrix. As the FM component increases, a reentrant phenomenon of the FM phase into the CO phase ($dH_c/dT>0$) is observed in the *H-T* phase diagram due to partial FM polarization. Also, in $Sm_{0.15}Ca_{0.85}MnO_3$, partial FM polarization explains the relatively low value of H_c. However, the physical origin of these behaviors is very different. For $Pr_{2/3}Ca_{1/3}MnO_3$, the CO/FM coexistence is due to the narrowing of the one-electron bandwidth, which favors CO against the classical FM *M* phase involved at this hole concentration. For the electron-doped systems the situation is less clear.

The low-field phase diagram of electron-doped systems presents similar features as those of $L_{1-x}Ca_xMnO_3$-based manganites. CG and OO/CO phases also occur for L = La, Pr, Th, or Bi.[13–15,18,23] The main difference between these two phases concerns the occurrence of concomitant orbital ordering with a structural transition from orthorombic to monoclinic structures for the second. In that case, the orbital degeneracy of e_g electrons is lifted, while they remain degenerate in CG phases. The CG-OO transition occurs when the concentration of e_g electrons is sufficient to produce a reduction of the lattice energy through its deformation with their localization. This scenario seems to be consistent with recent theoretical calculations taking into account the orbital degeneracy.[30] Thus the main parameter that governs the transition from the CG to the OO phase is the carrier concentration. Experimentally, the critical carrier concentration (x_c) lies always in the same range (0.1–0.15).[23] As a second-order parameter, the lattice distortion due to different cationic average size ($\langle r_A\rangle$), i.e., the one-electron bandwidth determined by the angle of the Mn-O-Mn bonds, will slightly modify the critical concentration: an increase of r_L induces a small decrease of x_c.[14] Another parameter that could influence the critical value is the orbital order itself, as well as the CO crystal. It is not clear how it evolves with *x*. As an example, two models of CO are proposed for $L_{1/3}Ca_{2/3}MnO_3$.[19,31] The definition of the orbital-ordering scheme and crystalline structure between $x=1/2$ and x_c deserves much more work in order to have a clear picture, and to understand the relevance of these parameters for the phase diagrams.

In summary, we have investigated the magnetic properties of electron-doped $Sm_{1-x}Ca_xMnO_3$ systems. The phase diagram in the *H-T* plane has been obtained. Field-induced transitions have been observed. They correspond to the melting of the OO with *C*-type AFM for $x=0.8$, and to the melting of CO for $x=3/4$ and below. With decreasing electron concentration, at the transition from the OO to the CG regime, $x\sim0.85$, the magnetization curves combine the two adjacent characteristic behaviors, giving macroscopic evidence of phase separation.

ACKNOWLEDGMENTS

The Belgian IUAP and the Flemish FWO programs have supported this work.

*Corresponding author. Email address: respaud@insa-tlse.fr

[1] J. M. D. Coey, M. Viret, and S. von Molnar, Adv. Phys. **48**, 167 (1999).
[2] M. Imada, A. Fujimori, and Y. Tokura, Rev. Mod. Phys. **70**, 1039 (1998).
[3] Y. Tokura and N. Nagaosa, Science **288**, 462 (2000).
[4] A. Moreo, S. Yonuki, and E. Dagotto, Science **283**, 2034 (1999).
[5] C. Zener, Phys. Rev. **82**, 403 (1951).
[6] Z. Jirák, S. Krupicka, Z. Šimša, M. Dlouhá, and S. Vratislav, J. Magn. Magn. Mater. **53**, 153 (1985); J. B. Goodenough, Phys. Rev. **100**, 564 (1955).
[7] H. Kawano, R. Kajimoto, H. Yoshizawa, Y. Tomioka, H. Kuwahara, and Y. Tokura, Phys. Rev. Lett. **78**, 4253 (1997).
[8] M. Tokunaga, N. Miura, Y. Tomioka, and Y. Tokura, Phys. Rev. B **57**, 5259 (1998); **60**, 6219 (1999).
[9] M. Respaud, A. Llobet, C. Frontera, C. Ritter, J. M. Broto, H. Rakoto, M. Goiran, and J. L. Garcia-Muñoz, Phys. Rev. B **61**, 9014 (2000).
[10] A. P. Ramirez, P. Schiffer, S. W. Cheong, C. H. Chen, W. Bao, T. T. M. Palstra, P. L. Gammel, D. J. Bishop, and B. Zegarski, Phys. Rev. Lett. **76**, 3188 (1996).
[11] Y. Murakimi, D. Shindo, H. Chiba, M. Kikuchi, and Y. Syono, Phys. Rev. B **59**, 6395 (1999).
[12] Y. Su, C. H. Du, P. D. Hatton, S. P. Collins, and S. W. Cheong, Phys. Rev. B **59**, 11 687 (1999).
[13] M. Hervieu, A. Barnabé, C. Martin, A. Maignan, F. Damay, and B. Raveau, Eur. Phys. J. B **8**, 31 (1999).
[14] C. Martin, A. Maignan, M. Hervieu, and B. Raveau, Phys. Rev. B **60**, 12 191 (1999).
[15] M. Hervieu, C. Martin, A. Maignan, G. Van Tendeloo, and B. Raveau, Eur. Phys. J. B **10**, 397 (1999).
[16] V. Kiryukhin, D. Casa, J. P. Hill, B. Keimer, A. Vigilante, Y. Tomioka, and Y. Tokura, Nature (London) **386**, 813 (1997).
[17] D. E. Cox, P. G. Radaelli, M. Marezio, and S. W. Cheong, Phys. Rev. B **57**, 3305 (1998).
[18] H. L. Liu, S. L. Cooper, and S. W. Cheong, Phys. Rev. Lett. **81**, 4684 (1998).
[19] S. Mori, C. H. Chen, and S. W. Cheong, Nature (London) **392**, 473 (1998).
[20] M. Respaud, J. M. Broto, H. Rakoto, M. Goiran, A. Llobet, C. Frontera, J. L. Garcia Muñoz, and J. Vanacken, J. Magn. Magn. Mater. **211**, 128 (2000).
[21] J. Hejtmánek, Z. Jirák, M. Maryško, C. Martin, A. Maignan, M. Hervieu, and B. Raveau, Phys. Rev. B **60**, 14 057 (1999).
[22] C. Martin, A. Maignan, F. Damay, M. Hervieu, and B. Raveau, J. Solid State Chem. **134**, 198 (1997).
[23] A. Maignan, C. Martin, F. Damay, and B. Raveau, Chem. Mater. **10**, 950 (1998).
[24] A. Maignan, C. Martin, F. Damay, B. Raveau, and J. Hejtmanek, Phys. Rev. B **58**, 2758 (1998).

[25] C. Martin, A. Maignan, M. Hervieu, B. Raveau, Z. Jirák, A. Kurbakov, V. Trounov, G. André, and F. Bourée, J. Magn. Magn. Mater. **205**, 184 (1999).
[26] C. Martin, A. Maignan, M. Hervieu, B. Raveau, Z. Jirák, M. M. Savosta, A. Kurbakov, V. Trounov, G. André, and F. Bourée, Phys. Rev. B **62**, 6442 (2000).
[27] C. Martin *et al.* (unpublished).
[28] R. Mahendiran, M. R. Ibarra, A. Maignan, F. Millange, A. Arulraj, R. Mahesh, B. Raveau, and C. N. R. Rao, Phys. Rev. Lett. **82**, 2191 (1999).
[29] J. L. Garcia Muñoz, M. Respaud, C. Frontera, A. Llobet, J. M. Broto, H. Rakoto, and M. Goiran, J. Appl. Phys. **85**, 5570 (1999).
[30] J. van den Brink and D. Khomskii, Phys. Rev. Lett. **82**, 1016 (1999).
[31] P. G. Radaelli, D. E. Cox, L. Capogna, S.-W. Cheong, and M. Marezio, Phys. Rev. B **59**, 14 440 (1999).